

Effect of the reaction medium on the progression of NaBH₄ hydrolysis reaction on fcc Co surfaces: A DFT study

N. KARAKAYA AKBAŞ* and B. KUTLU**

*Gazi University, Institute of Science, Department of Physics, Ankara, TURKEY

**Gazi University, Faculty of Science, Department of Physics, Ankara, TURKEY

Abstract

In this study, the effect of the reaction medium on the initial hydrogen decomposition of the NaBH₄ hydrolysis reaction in the presence of the Co catalyst surface has been theoretically investigated using the CASTEP package program based on density functional theory. The main purpose of the research is to distinguish the catalytic effects of fcc cobalt surfaces on the decomposition of hydrogen from NaBH₄ and to determine the effects of the environments formed by the hydrolysis of water at the most efficient cobalt surface on hydrogen decomposition. Therefore, the common surface types Co(111), Co(110), and Co(100) surfaces of the fcc cobalt crystal were used to determine the effect of fcc surface structure on hydrogen decomposition from NaBH₄ and water decomposition. The activation energies required for hydrogen decomposition from NaBH₄ on the catalyst surface of Co(111) with the lowest activation barrier were determined for each possible reaction medium containing different concentrations of H^{*} atoms, ·OH^{*} radicals, and H₂O^{*} molecules. The variation of the activation energies calculated for the reaction paths chosen for different amounts of H^{*} atoms and ·OH^{*} radicals are in good agreement with experimental expectations. According to our results, the value of activation energy increases as the ratio of ·OH^{*} radicals increases.

Introduction

As a result of traditional methods used in energy consumption, environmental pollution has shown that it is very important to use clean energy sources instead of fossil fuels that cause global warming. One of the alternative sources of clean energy to carbon-based fuels is hydrogen. Although hydrogen has a higher energy density per unit mass than gasoline, the volumetric energy density is quite low. Because of this reason, various techniques to store hydrogen such as compressed-cryogenic tanks and sorbent materials that exploit physical interactions are far from fulfilling the requirements [1-3]. Chemical hydrides are promising materials that hold hydrogen at room temperature through chemical bonds [3]. Although water

is an important source for hydrogen production, metal borohydrides (MBH₄) contains more hydrogen than water, so recent studies on hydrogen production have focused on the hydrolysis reaction of 1 mol of metal borohydride in 2 moles of water. This reaction is capable of producing 4 moles of H₂. Recently, experimental studies on the production of hydrogen from metal borohydrides (MBH₄) have shown that the hydrolysis rate of catalytic MBH₄ reactions depends on the proportion of ·OH radicals released from the decomposition of water [4,5]. So far, relatively few amounts of research have considered this effect clearly from the theoretical manner [6,7].

Sodium borohydride (NaBH₄), as a chemical hydride, can provide relatively high theoretical hydrogen yield (10.8 wt%) via hydrolysis reaction [8], which proceeds in an aqueous medium with a catalyst [9,10]. Studies to date have shown that hydrogen production by hydrolysis reaction of the NaBH₄ in aqueous solution has many advantages, such as high gravimetric and volumetric hydrogen capacity, stability in alkali state media, hydrogen production even at 0 °C and controllability of hydrogen generation via a catalyst. Moreover, the reaction can be recycled, the reaction rate is easy to control, and the hydrogen is generated with high purity [6, 9, 11-15].

Thermolysis [16], hydrolysis [4], and their simultaneous consideration in the same reaction medium [17,18] are available methods for the hydrogen release stored in NaBH₄. Among these methods, only the hydrolysis method has been considered for practical hydrogen production [12,19]. The hydrolysis of NaBH₄ was defined as early as 1953 by Schlesinger et al. [4]. The ideal NaBH₄ hydrolysis reaction is defined as;

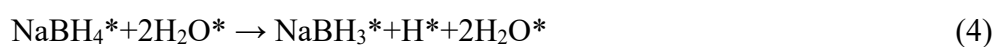


Experimental results show that sodium metaborate is highly stable during the reaction and also increases the pH of the solution due to water decomposition. In recent years, experimental studies have shown that Co is one of the most active metal catalysts for the NaBH₄ hydrolysis reaction of [4,20]. To date, studies on this reaction have shown that the reaction is exothermic and hence needs no energy input. The products (metaborates) of reaction are environmentally safe. The volumetric and gravimetric hydrogen storage efficiencies are high compared to other chemical hydrides and pure H₂ can be generated even at low temperatures [21]. The Co-based catalysts have good catalytic performance and there are considerable experimental studies have been conducted until today. Also, some researches emphasize the importance of cycle counts for catalyst and rate of degradation in practical uses of hydrogen storage. In this context, during

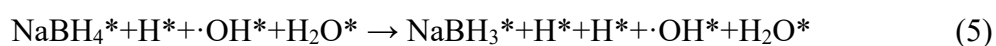
the literature search for catalyst research, in addition to the high activity of Co-based catalysts, the different advantages of these properties were taken into consideration. As is known, metallic Co is in the hcp phase at low temperatures and fcc phase at temperatures above 450 °C [22]. However, studies to date have shown that fcc Co surfaces are obtained at room temperature using nanoparticle production techniques [23, 24], and coating techniques [25]. Also, for bulk cobalt, the thermodynamically favored structure is the hcp structure, but for Co crystallites smaller than 20 nm, i.e. in the relevant size regime for Co Fischer-Tropsch synthesis (FTS) catalysts [26], the fcc structure is thermodynamically most favorable[27].

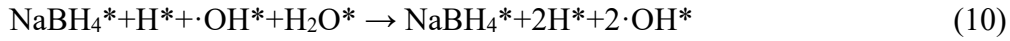
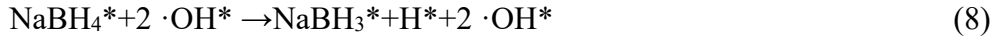
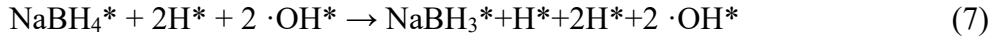
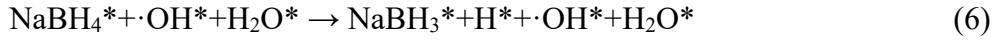
Also, water used in the production of hydrogen is a requirement in terms of the solubility of reactants and by-products. Understanding the reaction kinetics by reducing the amount of water on the pathway to obtaining NaBO₂ during the reaction of NaBH₄ with water is important to achieve the high energy density of the hydrogen storage system. The coherence between the theoretical and experimental studies guides development of new hydrogen storage materials and research of their catalytic activity. It should be considered that the differences of experimental investigations, such as molarities of reactants, temperature, etc., prevent an actual comparison with theoretical studies however they still give hints for the new researches.

One of the aims of this study is to determine the preferable cobalt surface for the first step of NaBH₄ hydrolysis reaction and decomposition of water. For this purpose the reactions as shown in Eqs. 2-4 are optimized on Co(111), Co(110), and Co(100) surfaces.



The second aim of this study is to investigate the effects of H^{*} atom and ·OH^{*} radical and H₂O^{*} molecule to the NaBH₄^{*} hydrolysis reaction on Co (111) surface. For this purpose, activation energies of the first step, which may have different possibilities, of the catalytic NaBH₄^{*} hydrolysis reaction on the surface were determined using DFT calculations in the presence of H^{*} atoms, ·OH^{*} radicals, and H₂O^{*} molecules. It is possible to define the first step in the sodium borohydride hydrolysis reaction on the Co (111) surface by the following reaction equations to create different medium conditions.





The symbol * in the reactions given above indicates that atoms and molecules interact with the catalytic surface. Eqs. 3-8 from these proposed reaction equations correspond to different reaction combinations for the first reaction step, where one of the hydrogens in NaBH_4^* decomposes. The last two are related to the decomposition of water. In this study, the effect of possible environmental conditions on the decomposition of one of the hydrogen in NaBH_4^* during the hydrolysis reaction of NaBH_4^* was theoretically investigated.

Computational Method

In this study, calculations were made using the CASTEP simulation package [28,29], which is a DFT code. The generalized gradient approach (GGA) is used by Perdew-Burke-Ernzerhof (PBE) with the potential for exchange-correlation [30, 31]. For fcc-bulk cobalt, our calculated value of lattice parameter for fcc Co is 3.57 Å, which is in good agreement with the 3.55 Å measured by phonon dispersion of the high temperature (833 °K) fcc phase of pure cobalt with intellectual neutron scattering [32]. The optimizations of the molecules were carried out in 3-d free space using spin-polarized total energy calculations.

First of all the Co(111), Co(110), and Co(100) surfaces were modeled using a four-layer slab in a (3x3) unit cell with the top two layers allowed to relax and the bottom two layers constrained to the bulk positions. Then, the cobalt surfaces, the geometric structures of the molecules on the cobalt surfaces, and the initial states and final states of the reactions in the Eqs. 2-4 reaction steps were optimized. After that, transition state calculations were performed of these reactions.

All calculations were performed using cutoff energy of 500 eV. Reciprocal space integration over the Brillouin zone was approximated with a finite sampling of k-point using the Monkhorst–Pack scheme and the k-point spacing was set to be 4x4x1. The structures were relaxed using a Broyden–Fletcher–Goldfarb–Shanno (BFGS) scheme with the following

convergence parameters for energy, force, displacement and stress are 5.0×10^{-5} eV/atom, 0.1 eV/Å, 0.005 Å, and 0.2 GPa, respectively. The slabs were separated from their periodic images by a vacuum width of 20 Å. Spin-polarization was considered to characterize the ferromagnetic structure of the metal.

The simplest way to determine intrinsic energy changes in the reaction medium of any reaction step is to identify the changes in energy barriers (activation energy) and reaction energies. The reaction energy (ΔH) for any reaction step was calculated using the Eq. 11,

$$\Delta H = E_{P/S} - E_{R/S} \quad (11)$$

where $E_{R/S}$ and $E_{P/S}$ are the total energy of the reactant and product molecules on the surface, respectively. The reaction is exothermic for the negative value of ΔH , otherwise it is endothermic.

The values of the forward (E_{FA}) and reverse (E_{RA}) activation energies were determined using the total energy values of the transition state, the reactant, and product molecules on the surface. The values of E_{FA} and E_{RA} are calculated by

$$E_{FA} = E_{TS/S} - E_{R/S} \quad (12)$$

and

$$E_{RA} = E_{TS/S} - E_{P/S} \quad (13)$$

the most important process in determining the activation energy for a reaction step is the determination of the transition state with minimum energy.

In a recent study, activation energy values were successfully obtained by performing transition states (TS) search calculations to separate the BH_4 molecule on various metal (111) surfaces [33]. Therefore, we used TS search calculations to get the activation energy values for each reaction step in this study. The transition states (TS) were searched using the LST/QST method [34] in the CASTEP simulation package. First, the linear synchronous transit (LST) maximization was performed, followed by energy minimization in the directions conjugating to the reaction pathway. Second, the approximated TS was used to perform quadratic synchronous transit (QST) maximization, with conjugate gradient minimization performed. The cycle is repeated until a stationary point was located in this method [35].

Results and Discussion

Optimization results of H_2O and $NaBH_4$ in the gas phase

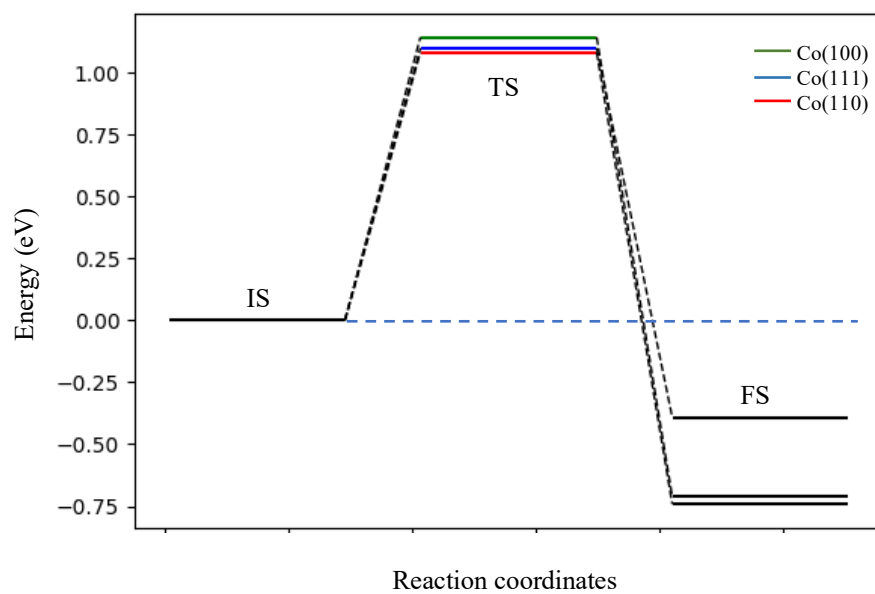
Structural parameters for isolated adsorbates in the gas phase, which are obtained by placing them in a large periodically repeated cubic box with sides of 15 Å are found via optimization. Firstly, we were calculated interatomic distance (d_{a-a}) and total energy for isolated molecules and along with the bond angle (α_{H-O-H}) of the H₂O molecule. The calculated d_{O-H} distance and α_{H-O-H} angle for molecular water are 0.97 Å (exp. 0.96 Å) and 104.59° (previous calc. 104.6°) respectively[36,37]. The d_{B-H} distance for NaBH₄ is 1.25 Å (exp. 1.22 Å) [38], for NaBH₃ is 1.21 Å and 1.20 Å, d_{O-H} distance for the OH molecule is 0.99 Å (exp. 0.97 Å) [39] and d_{H-H} distance for H₂ molecule is 0.75 Å (exp. 0.74 Å)[40]. Present results are in good agreement with the experimental results.

Transition state search calculations for fcc cobalt surfaces

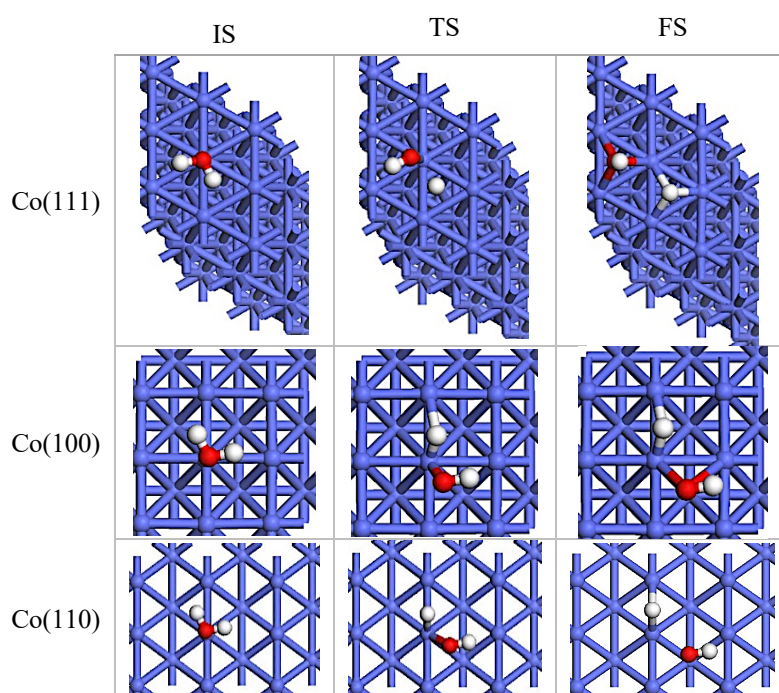
First of all, Co(111), Co(100), and Co(110) surfaces of metallic fcc cobalt, which is used as catalyst, were modeled by four layers of metals and a p(3x3) supercell. Initial and final states of possible decomposition reactions based on the main reaction are modeled and optimized separately for the surfaces. LST/QST transition state calculations were made using the initial and final states.

Table I. The values of E_{RB} , E_{PB} , and ΔH for reactions given by Eqs. 2-4. The optimizations were done for p(3x3) surface size on the fcc Co(111), (110), and (100) surface structures.

<i>Co(111) surface</i>	<i>$E_{RB}(eV)$</i>	<i>$E_{PB}(eV)$</i>	<i>$\Delta H(eV)$</i>
H ₂ O* → H* + OH*	1,100	1,492	-0,391
NaBH ₄ * → NaBH ₃ * + H*	0,263	0,632	-0,373
NaBH ₄ * + 2H ₂ O* → NaBH ₃ * + H* + 2H ₂ O*	0,214	1,063	-0,852
<i>Co(100) surface</i>			
H ₂ O* → H* + OH*	1,144	1,853	-0,711
NaBH ₄ * → NaBH ₃ * + H*	0,412	1,022	-0,609
NaBH ₄ * + 2H ₂ O* → NaBH ₃ * + H* + 2H ₂ O*	0,381	1,593	-1,212
<i>Co(110) surface</i>			
H ₂ O* → H* + OH*	1,082	1,824	-0,742
NaBH ₄ * → NaBH ₃ * + H*	0,407	0,981	-0,573
NaBH ₄ * + 2H ₂ O* → NaBH ₃ * + H* + 2H ₂ O*	0,374	1,704	-1,331

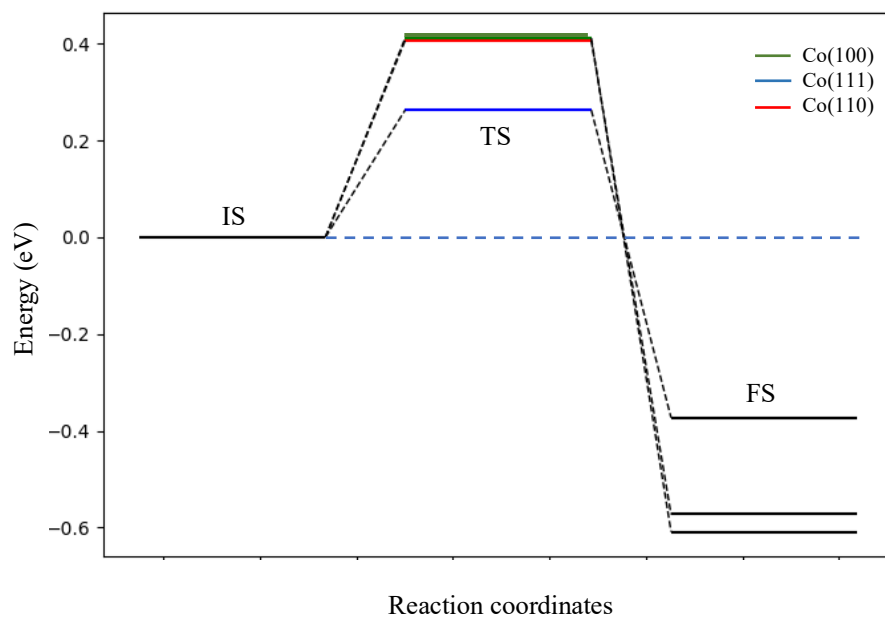


(a)

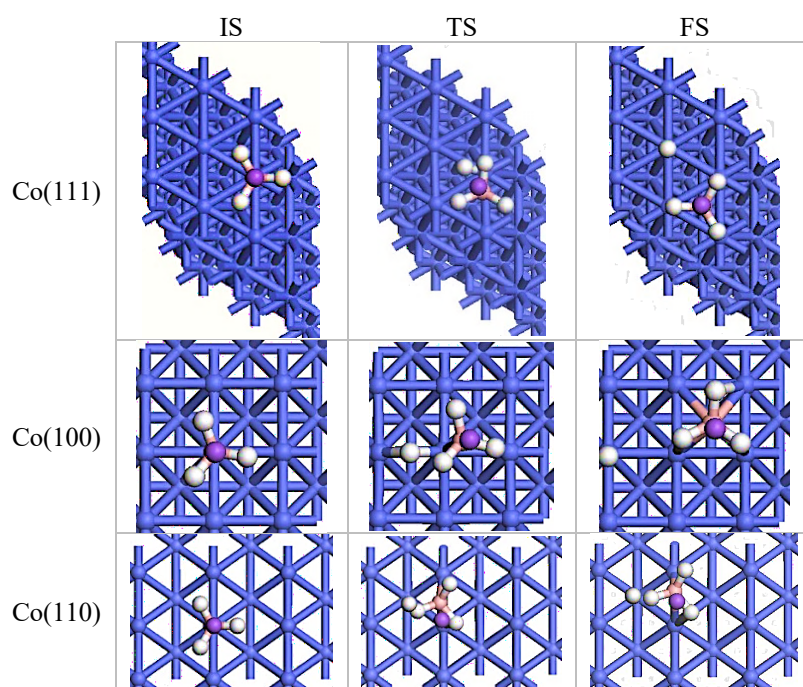


(b)

Fig.1 (a) Energy profile and (b) optimized structures of the IS, TS, and FS on the fcc Co surface for the $\text{H}_2\text{O}^* \rightarrow \text{H}^* + \text{OH}^*$ (Eqs. 2) reaction.

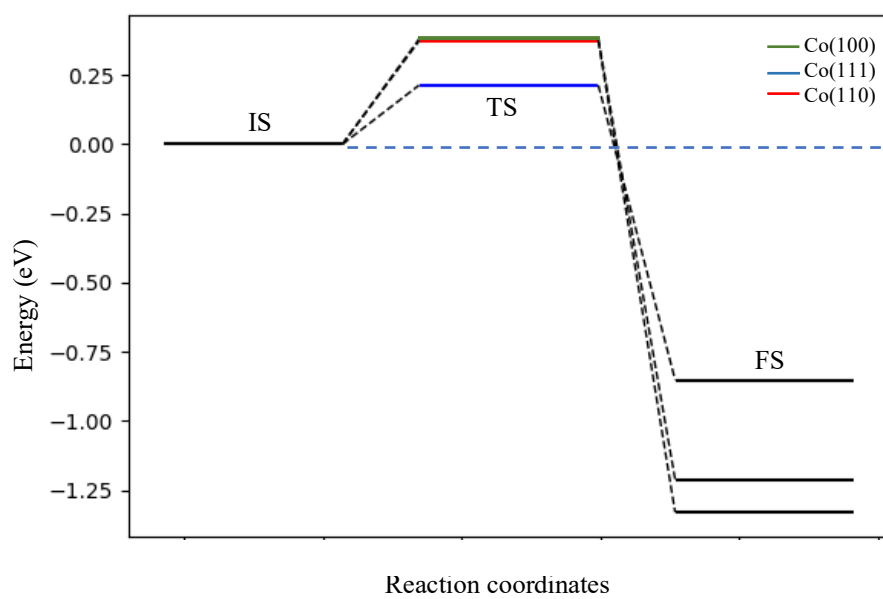


(a)

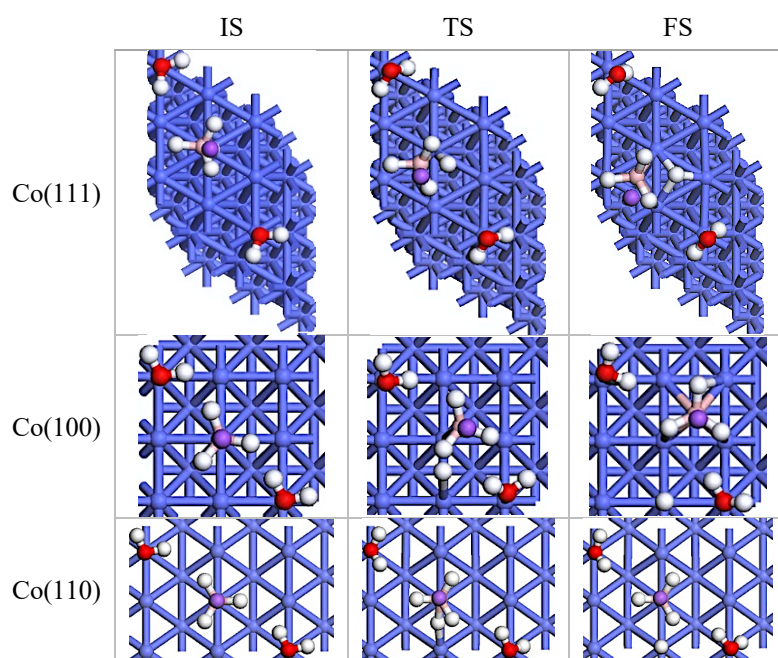


(b)

Fig.2 (a) Energy profile and (b) optimized structures of the IS, TS, and FS on the fcc Co surface for the $\text{NaBH}_4^* \rightarrow \text{NaBH}_3^* + \text{H}^*$ (Eqs. 3).



(a)



(b)

Fig.3 (a) Energy profile and (b) optimized structures of the IS, TS, and FS on the fcc Co surface for $\text{NaBH}_4^* + 2\text{H}_2\text{O}^* \rightarrow \text{NaBH}_3^* + \text{H}^* + 2\text{H}_2\text{O}^*$ (Eqs. 4).

LST/QST calculations do not differ in activation barrier values required for molecular water decomposition. And also; The values of energy required for hydrogen decomposition from NaBH_4 are shown in Table I for the anhydrous medium. As can be seen from Table I, the lowest activation energy for the decomposition of one of the hydrogen in NaBH_4^* in the aqueous and non-aqueous environment was obtained on the Co(111) surface. These results showed that the Co(111) surface from fcc Co surfaces is a preferred surface for catalytic effect in hydrogen separation from NaBH_4 . This result is in agreement with a study by Rostamikia et al.[41]. They calculated the activation barrier required for the decomposition of $\text{BH}_4^* \rightarrow \text{BH}_3^* + \text{H}^*$ on the Au(111) surface as 0.37 eV[41]. However, hydrolysis of water takes place at fcc Co surfaces with energies very close to each other. Therefore, it can be said that there is no preferred fcc Co surface for the hydrolysis of water.

Transition state search calculations for Co(111)-(4x4) surface

The calculations in this section are designed to determine the transition states of the reactions given in Equations (2-10). For the values of the parameters, the Co(111) surface was modeled using a four-layer (4x4) surface with the top two layers allowed to relax and the bottom two layers constrained to the bulk positions.

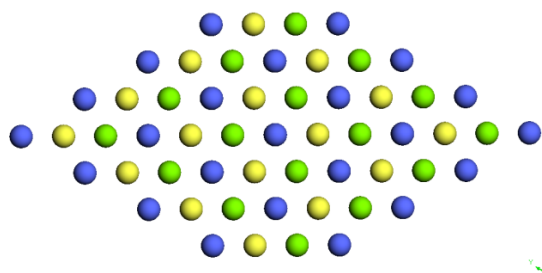


Fig.4 The possible adsorption sites of fcc Co surfaces. The positions of the top, bcc, and fcc are the blue, green, and yellow balls, respectively. The bridge position is the midpoint between the two blue balls.

There are four different adsorptive sites for Co(111)-(4x4) surface morphology; top, hcp, fcc, and bridge (shown in Fig.4). Before the TS search, the reactant and product molecules given in the reaction steps were optimized on the 4x4 surface. When the reactants and products of the reaction are optimized; NaBH_4^* , H_2O^* are adsorbed on top sites, NaBH_3^* is adsorbed

on the hcp site. In presence of other adsorbents, H^* and $\cdot\text{OH}^*$ adsorption sites are very high and weakly bound although H^* and $\cdot\text{OH}^*$ are adsorbed on top site of the clean surface.

To determine the effects of H_2O^* , $\cdot\text{OH}^*$ radical and H^* atom for the decomposition of NaBH_4 on the surface, we first obtained transition states for all reaction steps. As a result, we estimated the activation energies (E_A) corresponding to the forward activation barrier (E_{FA}) for the first step of the reaction pathway of formation of sodium metaborate from sodium borohydride.

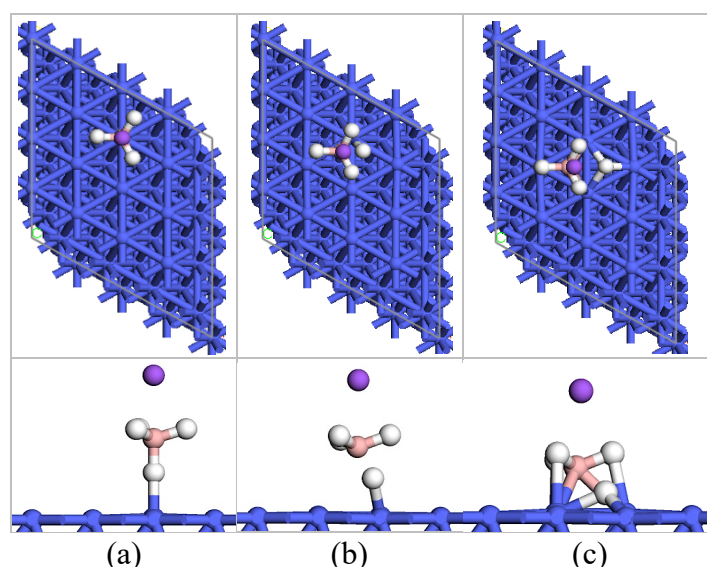


Fig.5 The optimized geometries of the molecular structures for the reaction step given by Eq.3 are shown; (a) the reactant, (b) the transition state, and (c) the product.

To determine the effects of $\cdot\text{OH}^*$ radicals formed by the decomposition of H_2O^* molecules, the activation energy was obtained for the reaction given by the Eq. (3) on the clean Co surface. The molecules of reactant (NaBH_4^*) and product ($\text{NaBH}_3^* + \text{H}^*$) on the surface were optimized. Fig.5(a), (b), and (c) shows the optimized geometries of the reactive (NaBH_4^*), TS, and product ($\text{NaBH}_3^* + \text{H}^*$) molecules on the surface.

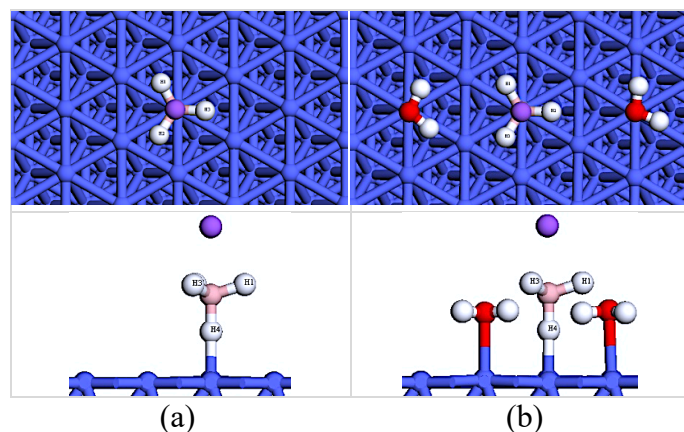


Fig.6 Optimized geometries of NaBH₄ molecule on the Co(111) surface in non-aqueous medium (a) and the presence of 2-mole water (b). (O, B, Na, H atoms are red, pink, purple, white respectively.)

As a result of the optimization, it was observed that the NaBH₄^{*} molecule has minimum energy at the top position while the positions of NaBH₃^{*} and H^{*} species after decomposition were configured to bound at the nearest fcc position and hcp position, respectively. NaBH₄ was optimized both in the presence and absence of water. It was seen that BH bond lengths in the NaBH₄ molecule have changed because of the interaction with the water. While the values of B-H1, B-H2, B-H3 bond lengths in the aqueous and anhydrous medium are 1.23 Å, the value of B-H4 bond length increases from 1.25 Å in the absence of water to 1.27 Å in the presence of water. This result indicates that water facilitates the separation of H from the NaBH₄ molecule.

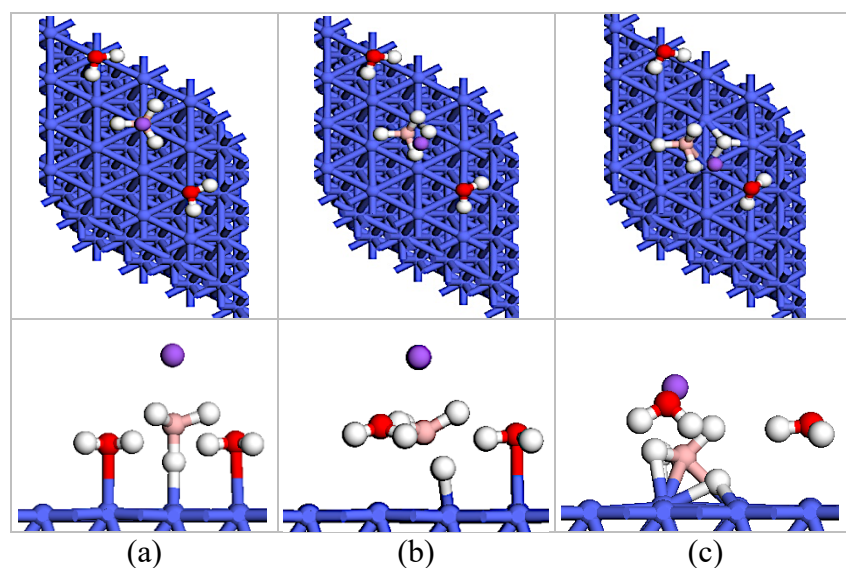


Fig.7 The optimized geometries of the molecular structures for (a) the reactant (b) the transition state and (c) the product on the Co(111) surface of the PW3 possible reaction pathway for the first reaction step.

On the other hand, the optimization result for the reaction in Eq.(4) which can be considered as the starting point of the reaction for 1 mol NaBH_4 molecule dissociation in 2 mol H_2O^* in the catalytic medium is given in Fig.7 (a), (b) and (c). While the activation energy for an H dissociation reaction from NaBH_4 on the clean Co(111) surface is 0.397 eV, it was calculated as 0.337 eV in the presence of 2 mol H_2O^* for the ideal hydrolysis reaction. Additionally, we investigated the hydrolysis reaction of sodium borohydride in the presence of $\cdot\text{OH}^*$ radicals and H^* atoms. The variation in numbers of H^* atoms and $\cdot\text{OH}^*$ radicals changes the energetic behavior of the relevant reaction step. This reaction design which can be seen in Eq. 4-10 represents different reaction media. It is very well known that half of the hydrogen atoms come from water decomposition in the hydrolysis reaction. It means that water molecules have to decompose and release H atoms and $\cdot\text{OH}$ radicals to the reaction medium.

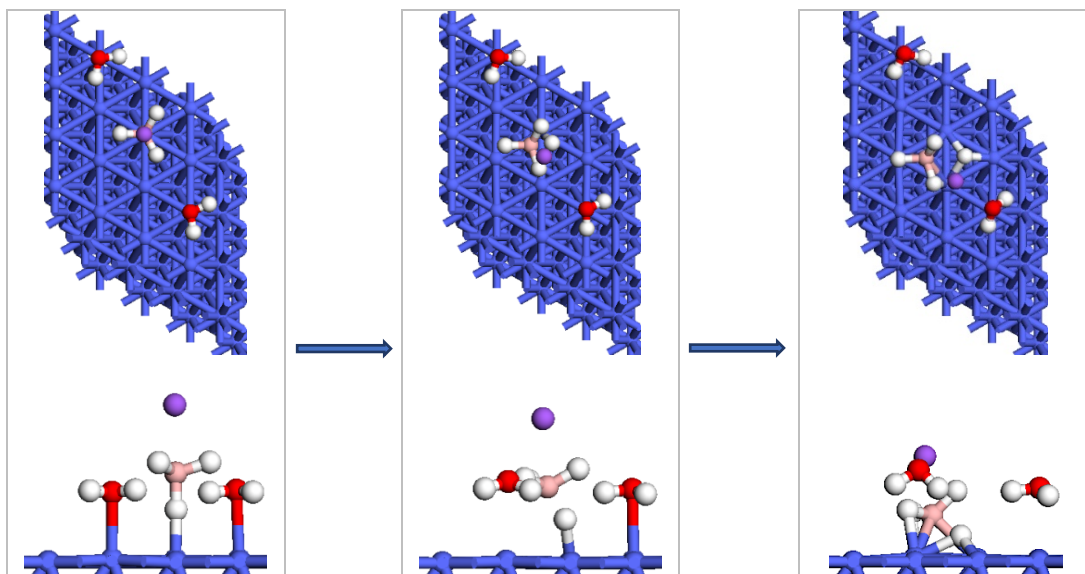
As seen in Table II, the reaction barrier energies for dissociation of H_2O^* molecule were calculated as 1,121 eV in the PW1 step for a clean surface, 0.98 eV, and 1.13 eV in the PW8 and PW9 steps for the reaction media, respectively. Our results are well compatible with the reaction barrier energies obtained for H_2O^* decomposition at different clean surfaces as 0.88 eV on Co(111) [42], 1.23 eV on Pd(100) [43], 1.04 eV on Fe(100) [44], 2.28 eV on Au(100) [45], 1.28 eV on Cu(111) [46], 0.92 eV on Rh(111) [37], 0.69 eV on Ni(111) [47] and 0.78 eV on Pt(111) [48]. The calculations of H_2O decomposition on different Co surfaces by F. F. Ma et al [42] showed that the reaction barrier for the O-covered Co surface is lower than the clean surface. Our results for the clean and non-clean Co surface supports the results of F.F. Ma et. al. [42]. Consistency of our results obtained for hydrolysis of water with the literature is an important support for the validity of the results obtained for the decomposition of NaBH_4 .

Table II. Reactant barriers, product barriers, and enthalpies of possible pathways for the first step of the hydrolysis reaction of NaBH₄ in the catalytic medium.

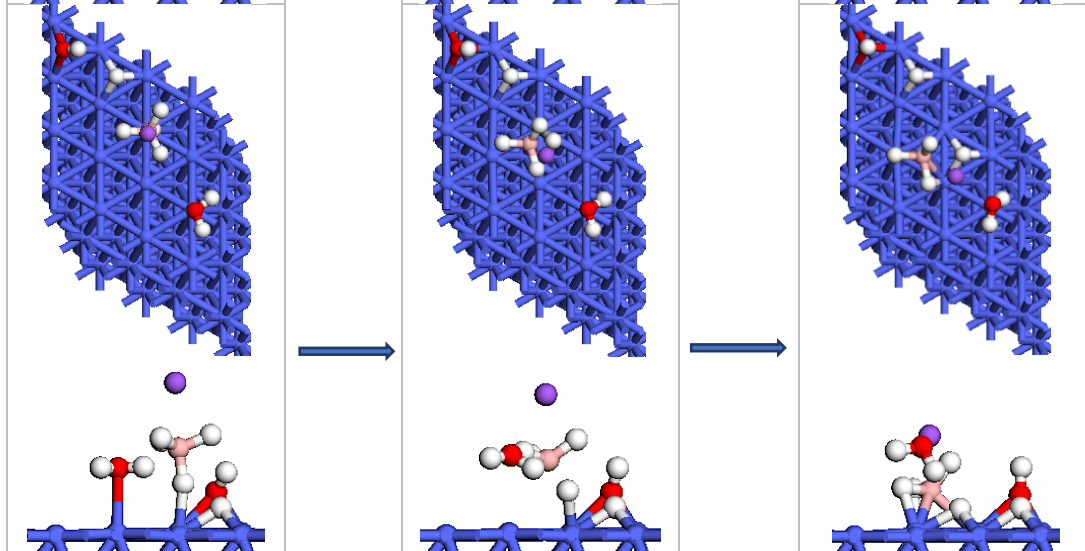
	Reactions	TS	E _{RB} (eV)	E _{PB} (eV)	ΔH(eV)
PW1	$\text{H}_2\text{O}^* \rightarrow \text{H}^* + \cdot\text{OH}^*$	TS1	1.121	1.511	-0.39
PW2	$\text{NaBH}_4^* \rightarrow \text{NaBH}_3^* + \text{H}^*$	TS2	0.397	1.130	-0.733
PW3	$\text{NaBH}_4^* + 2 \text{H}_2\text{O}^* \rightarrow \text{NaBH}_3^* + \text{H}^* + 2 \text{H}_2\text{O}^*$	TS3	0.337	1.997	-1.66
PW4	$\text{NaBH}_4^* + \text{H}^* + \cdot\text{OH}^* + \text{H}_2\text{O}^* \rightarrow \text{NaBH}_3^* + \text{H}^* + \text{H}^* + \cdot\text{OH}^* + \text{H}_2\text{O}^*$	TS4	0.354	2.013	-1.67
PW5	$\text{NaBH}_4^* + \cdot\text{OH}^* + \text{H}_2\text{O}^* \rightarrow \text{NaBH}_3^* + \text{H}^* + \cdot\text{OH}^* + \text{H}_2\text{O}^*$	TS5	0.374	2.185	-1.811
PW6	$\text{NaBH}_4^* + 2\text{H}^* + 2\cdot\text{OH}^* \rightarrow \text{NaBH}_3^* + \text{H}^* + 2\text{H}^* + 2\cdot\text{OH}^*$	TS6	0.610	1.334	-0.723
PW7	$\text{NaBH}_4^* + 2\cdot\text{OH}^* \rightarrow \text{NaBH}_3^* + \text{H}^* + 2\cdot\text{OH}^*$	TS7	0.691	1.135	-0.445
PW8	$\text{NaBH}_4^* + 2\text{H}_2\text{O}^* \rightarrow \text{NaBH}_4^* + \text{H}^* + \cdot\text{OH}^* + \text{H}_2\text{O}^*$	TS8	0.981	0.40	-0.581
PW9	$\text{NaBH}_4^* + \text{H}^* + \cdot\text{OH}^* + \text{H}_2\text{O}^* \rightarrow \text{NaBH}_4^* + 2\text{H}^* + 2\cdot\text{OH}^*$	TS9	1.134	0.573	-0.561

On the other hand, the transition state energies of the different atomic and molecular media to the hydrogen abstraction from NaBH₄ molecule are given in Table II and Fig.8., respectively. The PW3 step given in Table II is the most probable reaction at the beginning of the reaction. The other reaction steps show possible steps that may occur after the beginning of the reaction. In this study, TS values for H₂O* decomposition are in good agreement with the results of other studies, despite the different adsorbents on the surface. The cause of the TS9 being higher than the TS8 is due to the presence of excess ·OH* radicals in the medium in the PW9 reaction.

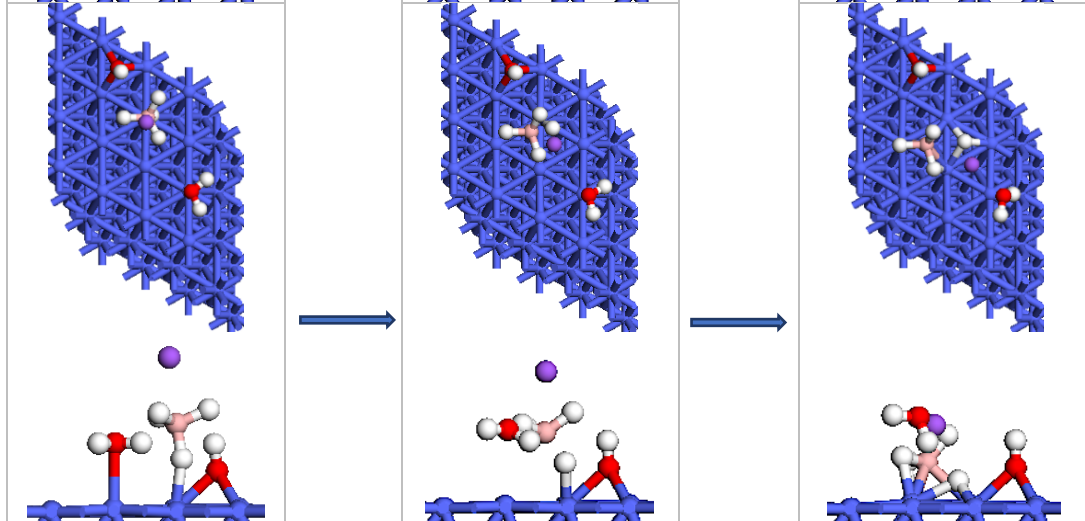
PW3



PW4



PW5



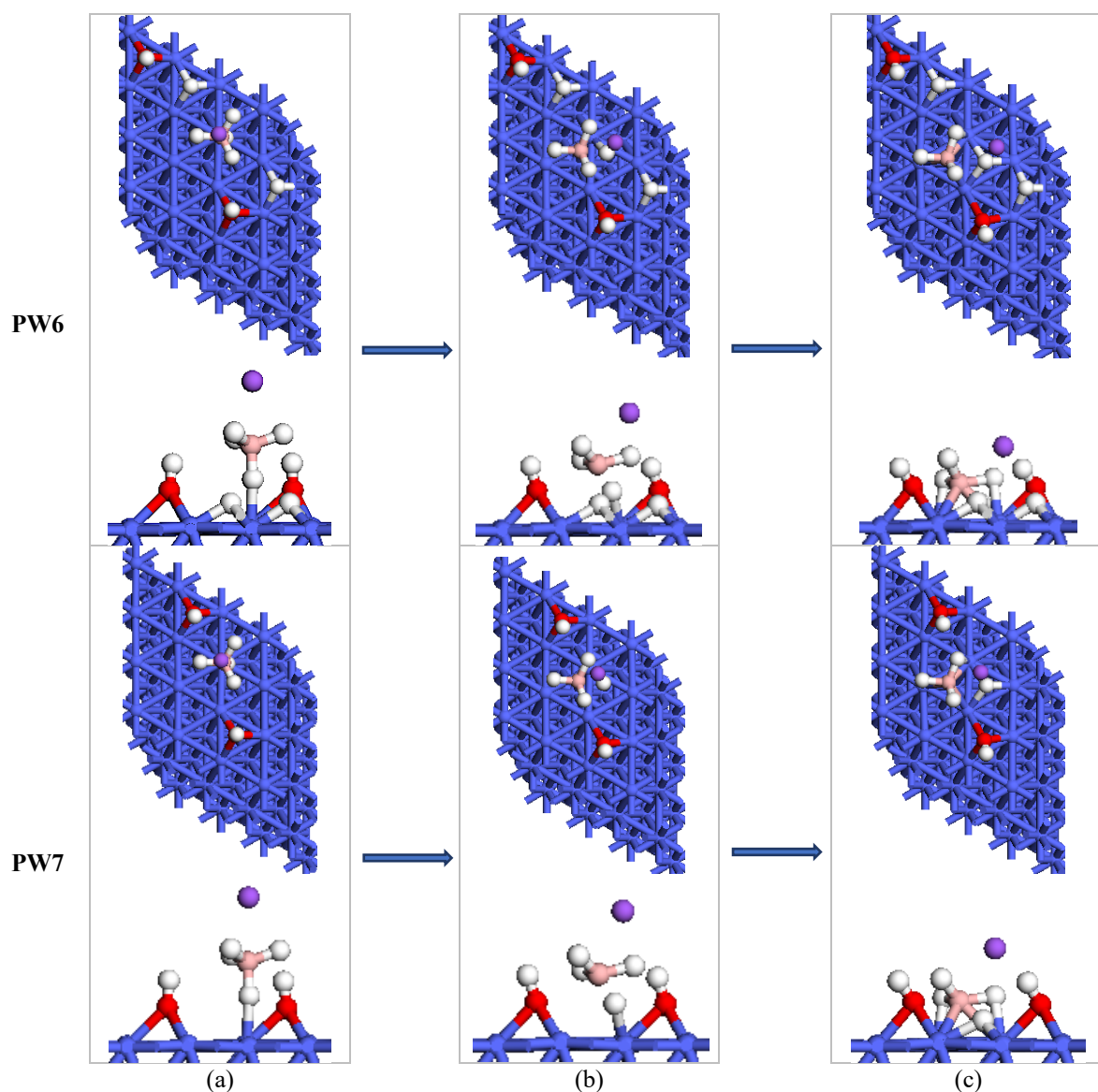


Fig.8. The optimized geometries of the molecular structures for (a) the reactant (b) the transition state and (c) the product on the Co(111) surface of the PW3-PW7 possible reaction pathways for the first reaction step.

The first step of the reaction is given in Eq. (1) was examined by the possible reaction paths PW3-PW7 for the dehydration of NaBH_4 for different $\cdot\text{OH}^*$ concentrations. In the PW3 reaction pathway where there are no $\cdot\text{OH}^*$, the energy barrier is 0.337 eV and reaction energy is -1.66 eV, while in the PW4 reaction where 1 mol H_2O^* is dissociated, the barrier is 0.354 eV and -1.67 eV. Reaction energies of the PW3 reaction pathway are -0.18 eV, 1.21 eV for Pt(111) and Au(111) respectively [7]. In the PW5 reaction pathway where an H^* atom is removed from the surface in the PW4 reaction pathway, the energy barrier increases to 0.374 eV. The energy barrier increased to 0.610 eV in the PW6 reaction path, where both H_2O^* molecules were

dissociated into $\cdot\text{OH}^*$ and H^* . The activation energy barrier increases with increasing $\cdot\text{OH}^*$ radical concentrations.

Conclusions

In this study, activation energies were obtained for possible reaction pathways for the separation of H from NaBH_4 molecule which is the first step in 1 mol NaBH_4 and 2 mol H_2O reaction using DFT calculations. The variation of activation energy (E_A) corresponding to these steps is given in Fig.9.

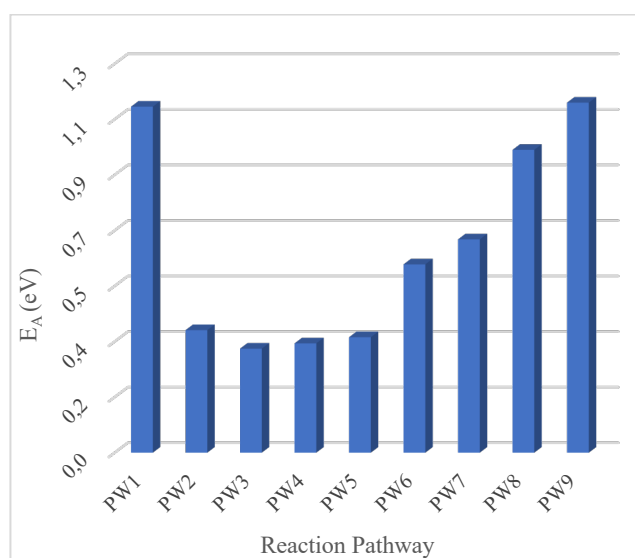


Fig.9. The variation of activation energy (E_A) corresponding to reaction pathways.

As can be seen in Fig.9, the activation energy is increased for further reaction steps. The increase in activation energy is due to the formation of the $\cdot\text{OH}$ radical in the reaction medium as a result of the decomposition of 2 mol H_2O . Acidic solutions have relatively more hydrogen ions, while alkaline (also called basic) solutions have relatively more hydroxyl ions. The acidity or alkalinity is determined by the amount of hydrogen ion (H^+) or hydroxyl (OH^-) in the medium. pH is the measurement of acidity or alkalinity of the aqueous solution [49]. The results obtained for the energy barrier indicate that the reaction rate decreases as the basicity of the medium increases. This is in good agreement with experimental studies conducted by S.S. Muir et al [6]. The activation energies calculated for the PW5 and PW7 reaction pathways are greater than those obtained for the PW4 and PW6 reaction pathways where the H^* atoms are present. This indicates that the acidity of the medium decreases as H^* atoms move away from the surface. For example, the activation energy for the PW4 is 0.354 eV, while for the PW5 it is 0.374 eV.

In this context, the change in the activation energies at the possible reaction stages are compatible with the concentration of the OH^- ions inversely proportional to the reaction rate. In other words, the change in the activation energy is thought to result from the change in the pH of the medium. Also, the activation energy for the clean surface is greater than that obtained for the surfaces containing H_2O^* , whereas it is smaller than that of the surfaces where water completely decomposes to $\cdot\text{OH}^*$ and H^* . This result indicates that the probability of formation of the first reaction step varies with the absorption of different molecules onto the catalytic surface. Moreover, the catalytic activity for the first reaction step is reduced by the absorption of different molecules onto the catalytic surface. Thus, it is possible to say that the $\cdot\text{OH}^*$ radicals are effective in determining the rate of the first step corresponding to the dissociation reaction of H atom from NaBH_4^* . The DFT calculation results for the separation of H^* atom from NaBH_4^* are in good agreement with the experimental results. The activation energy values obtained as a result of the transition state search calculations in the catalytic medium showed that the DFT calculations were distinctive in determining the effect of the intermediate states on the reaction rate.

Acknowledgment

All calculations in this article were carried out using the HPCC system provided by Gazi University.

References

1. M.P. Ramage, Transitions to Alternative Transportation Technologies; A Focus On Hydrogen, Washington, D.C., National Research Council; 2008. The National Academies Press. doi: 10.17226/12222.
2. U. Eberle, M. Felderhoff, F. Schuth, "Chemical and physical solutions for hydrogen storage", *Angew Chem. Int. Ed.*, 48(2009):6608-6630.
3. Fuel cell technologies office multi-year research, development and demonstration plan, in: Hydrogen storage, Washington, D.C., U.S. Department of Energy; 2012.
4. H.I. Schlesinger, H.C. Brown, A.E. Finholt, J.R. Gilbreath, H.R. Hoekstra, E.K. Hyde, "Sodium borohydride, its hydrolysis and its use as a reducing agent and in the generation of hydrogen", *J. Am. Chem. Soc.*, 75(1953):215-219.
5. A.M.F.R. Pinto, D.S. Falcão, R.A. Silva, C.M. Rangel, "Hydrogen generation and storage from hydrolysis of sodium borohydride in batch reactors", *Int. J. Hydrogen Energy*, 31(2006):1341-1347.
6. S.S. Muir, X. Yao, "Progress in Sodium Borohydride as a Hydrogen Storage Material: Development of Hydrolysis catalysts and reaction systems", *Int. Journal of Hydrogen Energy*, 36(2011): 5983-5997.
7. A.E. Genç, A. Akça, B. Kutlu, "The catalytic effect of the Au(111) and Pt(111) surfaces to the sodium borohydride hydrolysis reaction mechanism: A DFT study", *Int. J. Hydrogen Energy*, 43(2018):14347-14359.
8. I.P. Jain, P. Jain, A. Jain, "Novel hydrogen storage materials: a review of lightweight complex hydrides", *J. Alloy Compd.*, 503(2010):303-339.
9. R. Retnamma, A.Q. Novais, C.M. Rangel, "Kinetics of hydrolysis of sodium borohydride for hydrogen production in fuel cell applications: a review", *Int. J. Hydrogen Energy*, 36(2011):9772-9790.
10. Hydrogen and fuel cell program, 2007 annual progress report - IV. B.5a Development of an advanced chemical hydrogen storage and generation system, Washington, D.C., U.S. Department of Energy; 2007.

11. V. Kong, F. Foulkes, D. Kirk, J. Hinatsu, "Development of hydrogen storage for fuel cell generators. I: Hydrogen generation using hydrolysis hydrides", *Int. J. Hydrogen Energy*, 24(1999):665–675.
12. E.Y. Marrero-Alfonso, A.M. Beaird, T.A. Davis, M.A. Matthews., "Hydrogen generation from chemical hydrides", *Ind. Eng. Chem. Res.*, 48(2009):3703–3712.
13. L. Zhu, V. Swaminathan, B. Gurau, R.I. Masel, M.A. Shannon, "An onboard hydrogen generation method based on hydrides and water recovery for micro-fuel cells", *J. Power Sources*, 192(2009):556–561.
14. Y. Kojima, K.I. Suzuki, K. Fukumoto, Y. Kawai, M. Kimbara, H. Nakanishi, S. Matsumoto, "Development of 10 kW-scale hydrogen generator using chemical hydride", *J. Power Sources*, 125(2004):22–26.
15. D.M.F. Santos, C.A.C. Sequeira, "Sodium borohydride as a fuel for the future", *Renewable Sustainable Energy Rev.*, 15(2011):3980–4001.
16. E. Fakioğlu, Y. Yurum, N.T. Veziroğlu, "A review of hydrogen storage systems based on boron and its compounds", *Int. J. Hydrogen Energy*, 29(2004):1371-1376.
17. E. Shaffirovich, V. Diakov, A. Varma, "Combustion-assisted hydrolysis of sodium borohydride for hydrogen generation", *Int. J. Hydrogen Energy*, 32(2007):207-211.
18. V. Diakov, M. Diwan, E. Shaffirovich, A. Varma, "Mechanistic studies of combustion-stimulated hydrolysis of sodium borohydride for hydrogen generation", *Chem. Eng. Sci.* 62(2007):5586-5591.
19. E.Y. Marrero-Alfonso, J.R. Gray, T.A. Davis, M.A. Matthews, "Minimizing water utilization in the hydrolysis of sodium borohydride: the role of sodium metaborate hydrates", *Int. J. Hydrogen Energy*, 32(2007):4723-4730.
20. P.K. Singh, T. Das, "Generation of hydrogen from NaBH₄ solution using metal-boride (CoB, FeB, NiB) catalysts", *Int. J. Hydrogen Energy*, 42(2017):29360-29369.
21. S.C. Amendola, S.L. Sharp-Goldman, M.S. Janjua, N.C. Spencer, M.T. Kelly, P.J. Petillo, "A safe, portable, hydrogen gas generator using aqueous borohydride solution and Ru Catalyst", *Int. J. Hydrogen Energy*, 25(2000):969-675.
22. B.W. Lee, R. Alsenz, and A. Ignatiev, "Surface structures of the allotropic phases of cobalt", *Physical Review B*, 17(1978):1510-1520.

23. Q. Meng, S. Guo, X. Zhao, “Bulk metastable cobalt in the fcc crystal structure”, *Journal of Alloys and Compounds*, 580(2013):187-190.
24. E.A. Owen, D. Madoc Jones, “Effect of Grain Size on the Crystal Structure of Cobalt”, *Proc. Phys. Soc. B*, 67(1954): 456-466.
25. B.P. Tonner, Z.L. Han, and J. Zhang, “Structure of Co films grown on Cu(111) studied by photoelectron diffraction”, *Physical Review B*, 47(1993):9723-973.
26. G.L. Bezemer, J.H. Bitter, H.P.C.E. Kuipers, H. Oosterbeek, J.E. Holewijn, X. Xu, F. Kapteijn, A.J. van Dillen, K.P. de Jong, *J. Am. Chem. Soc.*, 128(2006):3956–3964.
27. O. Kitakami, H. Sato, Y. Shimada, F. Sato, M. Tanaka, “Size effect on the crystal phase of cobalt fine particles”, *Phys. Rev. B*, 56(1997):13849-13854.
28. M.C. Payne, M.P. Teter, D.C. Allan, T.A. Arias, J.D. Joannopoulos, “Iterative minimization techniques for ab initio total-energy calculations: molecular dynamics and conjugate gradients”, *Rev. Mod. Phys.*, 64(1992):1045-1097.
29. V. Milman, B. Winkler, J.A. White, C.J. Pickard, M.C. Payne, E.V. Akhmatkaya, R.H. Nobes, “Electronic Structure, Properties, and Phase Stability of Inorganic Crystals: A Pseudopotential Plane-Wave Study”, *Int. J. Quantum Chem.*, 77(2000): 895-910.
30. J.P. Perdew, K. Burke, M. Ernzerhof, “Generalized gradient approximation made simple”, *J. Physical Review Letters*, 77(1996): 3865–3868.
31. M.D. Segall, P.J.D. Lindan, M.J. Probert, C.J. Pickard, P.J. Hasnip, S.J. Clark, M.C. Payne, “First-principles simulation: ideas, illustrations, and the CASTEP code”, *Journal of Physics: Condensed Matter*, 14(2002): 2717-2744.
32. B. Strauss, F. Frey, W. Petry, J. Trampenau, K. Nicolaus, S.M. Shapiro, and J. Bossy, “Martensitic phase transformation and lattice dynamics of fcc cobalt”, *Phys. Rev. B*, 54(1996):6035-6038.
33. A. Akça, A.E. Genç, B. Kutlu, “BH₄ dissociation on various metal (111) surfaces A DFT study”, *Appl. Surf. Sci.*, 473(2019):681–692.
34. T.A. Halgren, W.N. Lipscomb, “The synchronous-transit method for determining reaction pathways and locating molecular transition states”, *Chem. Phys. Lett.*, 49(1977): 225–232.

35. S.G. Wang, X.Y. Liao, J. Hu, D.B. Cao, Y.W. Li, J.G. Wang, H.J. Jiao, "Kinetic aspect of CO₂ reforming of CH₄ on Ni(111): A density functional theory calculation", *Surf. Sci.*, 601(2007): 1271–1284.
36. CRC Handbook of Chemistry and Physics, in: D.R. Lide, 83rd ed., CRC Press LLC, New York, 2002.
37. M. Pozzo, G. Carlini, R. Rosei, D. Alfè, "Comparative study of water dissociation on Rh(111) and Ni(111) studied with first-principles calculations", *J. Chem. Phys.*, 126(2007): 164706(1-12).
38. P. Fischer, A. Züttel, "Order-disorder phase transition in NaBD₄". *Mater. Sci. Forum.*, 443-444 (2004): 287-290.
39. K.P. Huber, G. Herzberg, *Molecular Spectra and Molecular Structure*, in: IV. Constants of Diatomic Molecules, National Research Council of Canada, 1979.
40. B.H. Bransden, C.J. Joachin, *Physics of Atom and Molecules*, Wiley, New York, 1983.
41. G. Rostamikia, A.J. Mendoza, M.A. Hickner, M.J. Janik, *Journal of Power Sources*, 196 (2011):9228-9237.
42. F.F. Ma, S.H. Ma, Z.Y. Jiao, X.Q. Dai, "Adsorption and decomposition of H₂O on cobalt surfaces: A DFT study", *Appl. Surf. Sci.*, 384(2016):10–17.
43. Z. Jiang, L. Li, M. Li, R. Li, T. Fang, "Density functional theory study on the adsorption and decomposition of H₂O on clean and oxygen-modified Pd(100) surface", *App. Surf. Sci.*, 301(2014): 468-474.
44. R.R.Q. Freitas, R. Rivelino, F.B. Mota, C.M.C. Castilho, "Dissociative adsorption and aggregation of water on the Fe(100) surface: A DFT study", *J. Phys. Chem. C*, 116(2012):20306–20314.
45. Z. Jiang, M. Li, T. Yan, T. Fang, "Decomposition of H₂O on clean and oxygen-covered Au(100) surface: A DFT study", *Appl. Surf. Sci.*, 315(2014): 16–21.
46. Y.Q. Wang, L.F. Yan, G.C. Wang, "Oxygen-assisted water partial dissociation on copper: a model study", *Phys. Chem. Chem. Phys.*, 17(2015): 8231–8238.
47. A. Mohsenzadeh, K. Bolton, T. Richards, "DFT study of the adsorption and dissociation of water on Ni(111), Ni(110) and Ni(100) surfaces", *Surf. Sci.*, 627(2014):1–10.

48. J.L.C. Fajín, M.N.D.S. Cordeiro, J.R.B. Gomes, “Density functional theory study of the water dissociation on platinum surfaces: General trends”, *J. Phys. Chem. A*, 118(2014): 5832–5840.
49. R.D. Down, J.H. Lehr, “Environmental Instrumentation and Analysis Handbook, in: J.R. Gray, *pH Analyzers and Their Application*”, 2005, p:460.